BIOTECHNOLOGY

Very fast CRISPR on demand

Yang Liu[1]*, Roger S. Zou[2]*, Shuaixin He[1], Yuta Nihongaki[3], Xiaoguang Li[3], Shiva Razavi[2]†, Bin Wu[1,5,6]‡, Taekjip Ha[1,2,4,7]‡

CRISPR-Cas systems provide versatile tools for programmable genome editing. Here, we developed a caged RNA strategy that allows Cas9 to bind DNA but not cleave until light-induced activation. This approach, referred to as very fast CRISPR (vfCRISPR), creates double-strand breaks (DSBs) at the submicrometer and second scales. Synchronized cleavage improved kinetic analysis of DNA repair, revealing that cells respond to Cas9-induced DSBs within minutes and can retain MRE11 after DNA ligation. Phosphorylation of H2AX after DNA damage propagated more than 100 kilobases per minute, reaching up to 30 megabases. Using single-cell fluorescence imaging, we characterized multiple cycles of 53BP1 repair foci formation and dissolution, with the first cycle taking longer than subsequent cycles and its duration modulated by inhibition of repair. Imaging-guided subcellular Cas9 activation further facilitated genomic manipulation with single-allele resolution. vfCRISPR enables DNA-repair studies at high resolution in space, time, and genomic coordinates.

RNA-guided DNA targeting with CRISPR-Cas9 has revolutionized biomedical research for genome editing and beyond (*1*). After genomic DNA cleavage by Cas9, DNA damage response (DDR) proteins are recruited to initiate complex repair processes (*2*). Although DDR is known to be influenced by factors such as target sequence (*3*, *4*), cell cycle (*5*), and chromatin dynamics (*6*), the precise timing and sequence of cellular events require further investigation. Cas9 has potential as a tool to study the dynamics of DDR but currently lacks the necessary level of control to initiate precise DNA damage on demand. To unveil the sequence of Cas9-induced DDR events in living cells, an inducible Cas9 system with the spatiotemporal resolution that matches the rapidity and subcellularity of DDR would be powerful.

Numerous inducible Cas9 systems have been developed (*7*–*11*). However, these methods often exhibit compromised function in the engineered proteins, coarse temporal control in the hour time scale (because Cas9 still has to find the target after induction), and no spatial control or control at the millimeter length scale at best.

Here, we report a very fast CRISPR-Cas9 system (vfCRISPR) that allows genome editing on demand at the submicrometer space scale and the second time scale. Through synchronized double-strand break (DSB) induction followed by complementary biochemical, sequencing, and imaging-based assays, we characterized the early molecular events that underlie the initiation and progression of DNA repair with high spatiotemporal precision.

The design principle of vfCRISPR is based on the *Streptococcus pyogenes* Cas9 (Cas9 henceforth) cleavage mechanism. The protospacer adjacent motif (PAM)–proximal 9- to 10-bp region of guide RNA (gRNA) governs Cas9 binding to its target DNA, whereas additional base pairing at the PAM-distal region (10 to 20 bp) is required for cleavage (*12*, *13*). Mismatches in the PAM-distal region prevent full unwinding of target DNA (*14*) and conformational changes of the HNH domain (*15*) required for cleavage. On the basis of this mechanistic understanding, we replaced two or three uracils at the PAM-distal region of crRNA with light-sensitive, 6-nitropiperonyloxymethyl–modified deoxynucleotide thymine caged nucleotides (*16*), forming a caged gRNA (cgRNA) when hybridized to wild-type trans-activating CRISPR RNA (tracrRNA) (Fig. 1A). The Cas9/cgRNA complex retains the ability to bind its target DNA but cannot cleave because the steric hindrance imposed by the caging groups prevents full DNA unwinding and nuclease activation. Upon light stimulation at 365 or 405 nm, the caging groups are removed and the prebound, now-activated Cas9/cgRNA complex rapidly cleaves target DNA.

An electrophoretic mobility shift assay confirmed that Cas9/cgRNA stably bound to target DNA without light and no cleavage was observed (Fig. 1B). After uncaging with light, the Cas9/cgRNA complex efficiently cleaved DNA within seconds in vitro (Fig. 1, C and D, and fig. S1).

Next, we characterized the activity of vfCRISPR in human embryonic kidney 293 cells by targeting four endogenous loci and found light-induced indel efficiency up to 97%, whereas cells without light exposure had almost no detectable indels (Fig. 1E and fig. S2). Cells exposed to this dosage of light exhibited no apparent phototoxicity (fig. S3). Approximately 50% of DNA cleavage was found within 30 s after light activation (Fig. 1F and fig. S4). Compared with other Cas9 induction methods, vfCRISPR exhibited much faster cleavage kinetics and higher cleavage efficiency (*17*, *18*) (Fig. 1, G and H). We attribute the very fast kinetics to skipped nuclear localization or target-searching steps, and the higher cleavage efficiency to the use of wild-type Cas9. Genome-wide analysis of off-target editing using GUIDE-seq (*19*) also revealed reduced off-target activity compared with wild-type gRNA (fig. S5), consistent with improved specificity from deoxyribonucleotide incorporation into the guide RNA (*20*). These experiments demonstrated that cgRNA enables very fast and efficient inducible DNA cleavage in mammalian cells.

With a precisely defined time for cleavage, vfCRISPR allowed us to investigate the generation and repair kinetics of Cas9-mediated DSBs. We measured the percentage of DSBs and indels as a function of time after Cas9 activation at multiple target sites and adopted mathematical models to describe the kinetics of DSB and indel formation (*21*) (Fig. 1I, fig. S6, and supplementary materials, models I and II). Model fitting led us to hypothesize the recutting of +1 insertion DNA at *ACTB*, which we subsequently verified both in vitro and in cells through recutting of a monoclonal cell line with a pure +A indel product at *ACTB* (figs. S7 and S8).

Using highly synchronized DNA cleavage, we performed time-resolved chromatin immunoprecipitation followed by sequencing (trChIP-seq) to track the recruitment of MRE11, which forms the MRN complex with Rad50 and Nbs1, to the *ACTB* cleavage site (*18*) (Fig. 2A). We observed rapid MRE11 recruitment that reached half-maximal signal between 5 and 15 min (Fig. 2, B and C, and fig. S9A). This is slower than recruitment of another MRN component, Rad50, after laser microirradiation (*22*), potentially because of the delay in exposure of Cas9-induced DSBs (fig. S9B). Both ChIP-seq and probe-based ChIP-quantitative polymerase chain reaction (qPCR) detected the emergence of MRE11-bound DNA that spanned the cleavage site 15 min after Cas9 activation (Fig. 2, B and D, and fig. S10A). This spanning population, which we attribute to repaired DNA still bound by MRE11, was present across different target sequences and cell types (*18*) (fig. S10, B to D, and fig. S11). Inhibition of the catalytic subunit of DNA-dependent protein kinase (DNA-PKcs) with KU-0060648 led to a reduction in spanning fragments with a concomitant increase in fragments that ended

[1]Department of Biophysics and Biophysical Chemistry, Johns Hopkins University, Baltimore, MD, USA. [2]Department of Biomedical Engineering, Johns Hopkins University, Baltimore, MD, USA. [3]Department of Cell Biology, Johns Hopkins University, Baltimore, MD, USA. [4]Department of Biophysics, Johns Hopkins University, Baltimore, MD, USA. [5]The Solomon H. Snyder Department of Neuroscience, Johns Hopkins University, Baltimore, MD, USA. [6]The Center for Cell Dynamics, Johns Hopkins University, Baltimore, MD, USA. [7]Howard Hughes Medical Institute, Baltimore, MD, USA.
*These authors contributed equally to this work.
†Present address: Department of Biological Engineering, Massachusetts Institute of Technology, Cambridge, MA, USA.
‡Corresponding author. Email: tjha@jhu.edu (T.H.); bwu20@jhu.edu (B.W.)

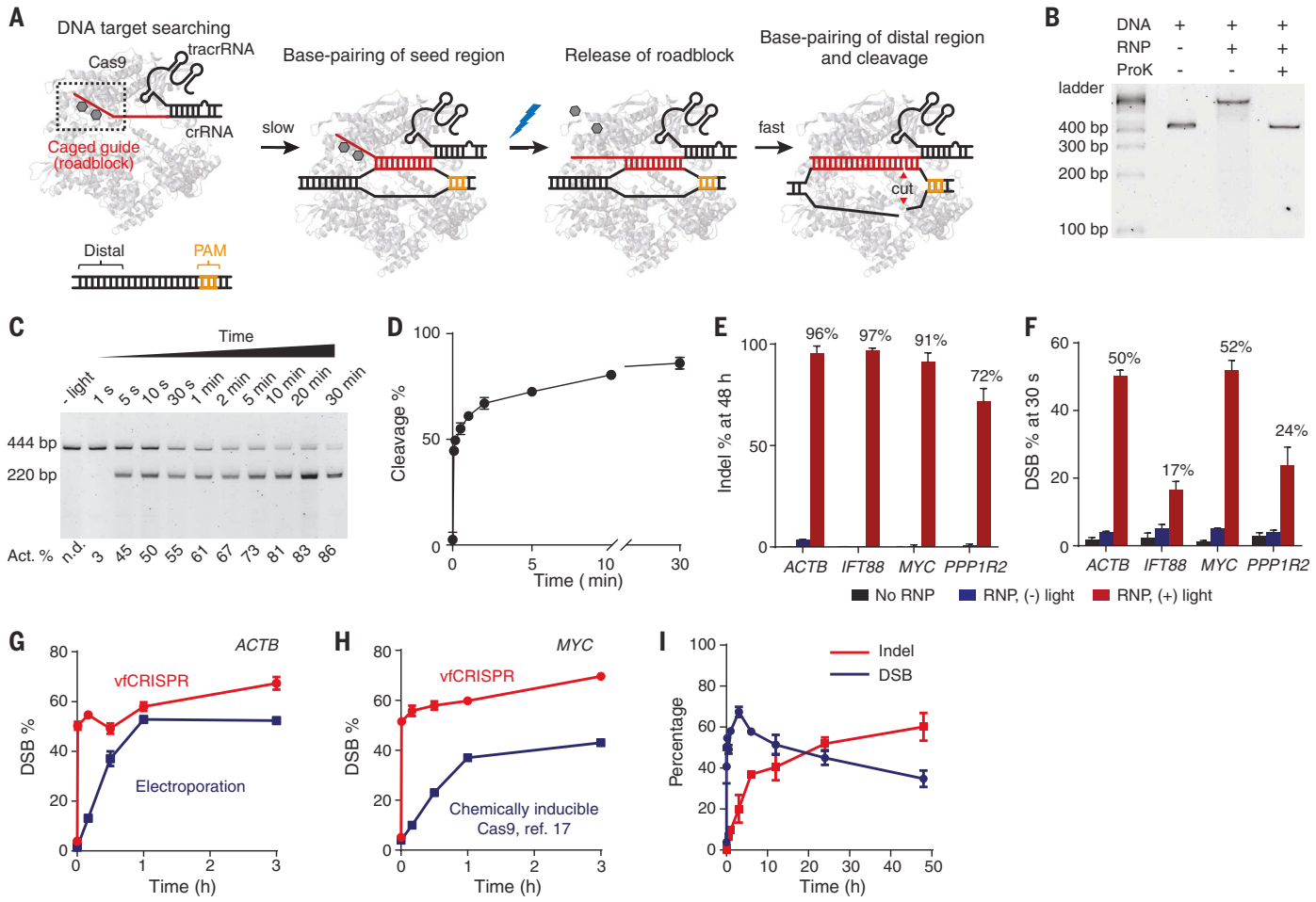

Fig. 1. Characterization of vfCRISPR in vitro and in cells. (**A**) Schematic of Cas9 activation by modulating base pairing between the PAM-distal region of cgRNA and genomic DNA. (**B**) Without light, Cas9/cgRNA ribonucleoprotein (RNP) bound to target DNA without cleavage, causing a clear band shift. Proteinase K degraded Cas9, causing target DNA to shift back to the original position. (**C** and **D**) Fast and efficient in vitro cleavage kinetics of Cas9 after light activation. (**E**) Indels detected by high-throughput sequencing of PCR-amplified genomic DNA extracted from cells without RNP, with RNP but no light, and with RNP 48 hours after light activation. (**F**) DSBs detected by DSB-droplet digital PCR of genomic DNA extracted from cells without RNP, with RNP but no light, and with RNP 30 s after light activation. (**G** and **H**) Percentage of DSBs over time using vfCRISPR (red) compared with either RNP electroporation [(G), target sequence at *ACTB*] or a chemically inducible system [(H), target sequence at *MYC*]. (**I**) DSBs and normalized indels (see the materials and methods) at *ACTB* over time after Cas9 activation.

at the cut site (Fig. 2E and fig. S12). Deep amplicon sequencing of spanning DNA revealed consistent 10 to 15% indels, whereas total indels rose from 2 to 20% within that period of time (Fig. 2F and fig. S13). Together, these results are consistent with transient MRE11 retention on ligated genomic DNA that was processed in a DNA-PKcs–dependent manner.

H2AX is known to be phosphorylated (γH2AX) for 1 to 2 Mb around a DSB undergoing active repair (*23*), but the dynamics of initial γH2AX spreading is unknown. trChIP-seq for γH2AX revealed rapid expansion of a "main peak" around the cleavage site at the speed of ~150 kb/min, reaching 8 Mb at 1 hour (Fig. 2, G and H, and fig. S14). Statistical testing (see the materials and methods) revealed another layer of γH2AX enrichment that expanded linearly at 460 kb/min and spanned up to 30 Mb at 1 hour (Fig. 2, I and J, and fig. S15). To our knowledge, γH2AX enrichment up to tens of megabases has not been previously reported. Although this may be a feature specific to Cas9-induced DSBs, synchronized, high-efficiency cleavage with vfCRISPR may have contributed to the detection of lower levels of enrichment.

Next, we performed single-cell fluorescence imaging to capture the dynamics of repair protein recruitment induced by vfCRISPR. To a monoclonal U-2 OS cell line stably expressing Cas9-EGFP, we cotransfected a truncated gRNA (11-mer in the protospacer) targeting a highly repetitive region in chromosome 3 (Ch3Rep) with a cgRNA targeting the *PPP1R2* gene, only 36 kb downstream of Ch3Rep (*24*–*26*). Upon light activation, a single DSB is generated at *PPP1R2*, which is fluorescently marked by an array of Cas9-EGFPs decorating Ch3Rep (Fig. 3A). We confirmed recruitment of multiple endogenous repair factors (pATM, MDC1, 53BP1, and γH2AX) to the single break sites (fig. S16, A to D). γH2AX foci size increased over time (fig. S16D), consistent with the γH2AX spreading reported by trChIP-seq.

To track real-time repair dynamics through live-cell imaging, we stably coexpressed 53BP1-mCherry (*27*) with Cas9-EGFP in U-2 OS cells (Fig. 3, A to C). Most of the Cas9-EGFP–labeled alleles colocalized with 53BP1-mCherry foci over the course of 8 hours after Cas9 activation (fig. S17A and movie S1), indicating efficient cleavage at *PPP1R2*. The onset time for 53BP1 recruitment (T_1) was heterogeneous between cells and alleles, with most foci appearing within 1 hour (Fig. 3D). Maximum likelihood estimation of a two-step mathematical model for T_1 yielded a DSB detection time (τ_d) of 12 ± 2.2 min and a Cas9 target-searching time (τ_s) of 43 ± 3.6 min (Fig. 4C and supplementary materials).

Each 53BP1 focus underwent a cycle of enlargement and dissolution, with most exhibiting more

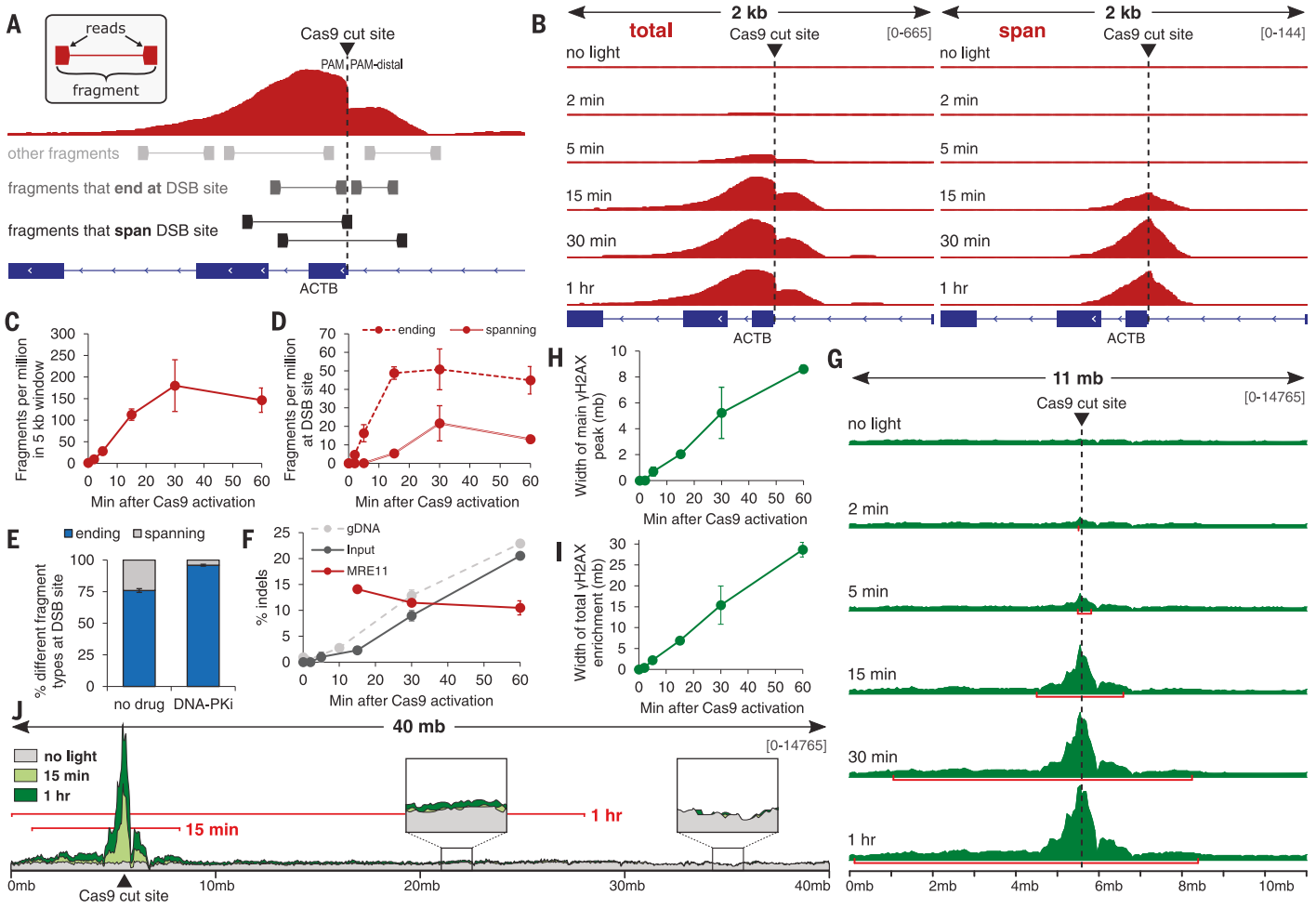

Fig. 2. trChIP-seq reveals dynamics of MRE11 recruitment and H2AX phosphorylation after synchronized Cas9-induced DSBs. (**A**) Schematic of MRE11 ChIP-seq analysis for paired-end reads. (**B**) Visualization of MRE11 peak features over time after Cas9 activation. The left column ("total") piles all fragments. The right column ("span") only piles fragments that span the cleavage site. (**C**) Fragments per million in the 5-kb window around the cleavage site over time. (**D**) Fragments per million that either span or start and/or end at the cleavage site over time. Fragments that start and/or end at the DSB site are enriched first, followed by an ~15-min delay by fragments that span the DSB site. (**E**) Proportion of fragments that span the DSB site that are depleted with DNA-PKcs inhibition. (**F**) Percentage of indels calculated from deep sequencing of PCR amplicons from both ChIP input (dark gray) and MRE11 ChIP (red) DNA that span the cleavage site. Indel kinetics from Fig. 1I are included for comparison (light gray, dashed, "gDNA"). (**G**) γH2AX enrichment over time in an 11-mb window around the cleavage site. Red bars mark the width of the "main" γH2AX peak detected using MACS2. (**H**) Width of the main γH2AX peak over time detected using MACS2. (**I**) Width of total enrichment detected using Student's *t* test with Bonferroni correction ($P < 0.05$) comparing no-light results with all after-activation results. (**J**) Illustration of enrichment up to ~30 mb along Chr7:1-40,000,000 ($P < 0.05$). Red bars mark the width of total γH2AX enrichment detected using Student's *t* test.

than one and up to five cycles over 8 hours, consistent with a previous report (*26*) (fig. S17B). The estimated τ_s and τ_d for subsequent rounds of 53BP1 recruitment agreed well with those for the first round, suggesting that each 53BP1 cycle corresponds to at least one repair event (Fig. 3E and table S6).

Duration of the initial 53BP1 cycle (D_1) was on average significantly longer than subsequent cycles (Fig. 3H). D_1 varied over a wide range and was positively correlated between two alleles in the same cell but not between different cells (Fig. 3, F and G, and figs. S18 and S19), suggesting that stochastic differences in chromatin environments between the two alleles is not the main reason for the large variation in D_1. Inhibition of ATM using KU-0055933 eliminated 53BP1 foci (fig. S20), consistent with its role as an upstream regulator of 53BP1 recruitment. Inhibition of DNA-PKcs prolonged 53BP1 foci without affecting 53BP1 recruitment (Fig. 3, H to J, and fig. S20), leading to fewer 53BP1 cycles and further supporting our interpretation that 53BP1 cycles mark successive rounds of DSBs and repair (figs. S21 to S23).

Finally, we extended vfCRISPR to spatially manipulate single genomic alleles. Both Ch3Rep alleles were bound by an array of Cas9/cgRNAs within the same nucleus. We focused a 405-nm laser beam to one Ch3Rep allele, which locally activated Cas9 to cleave the targeted allele while keeping the other one intact (fig. S24). Almost half of cells exhibited 53BP1 recruitment to the targeted allele within 1 hour, whereas only 6% of cells showed recruitment to both alleles, showing single-allele specificity (Fig. 4, A and B, and movie S2). We also demonstrated allele-specific manipulation of a nonrepetitive cleavage site at *PPP1R2* (Fig. 4, C and D, and movie S3). We observed only one round of 53BP1-mCherry recruitment, likely because only one round of cleavage was possible owing to the activation of only a small subset of Cas9/cgRNA in the nucleus (fig. S25). Laser beam alone was not responsible for 53BP1 recruitment (fig. S26), and conditions were optimized to maximize single-allele specificity, which was 80% or higher for both experimental schemes (Fig. 4, B and D). The capability of vfCRISPR to manipulate single genomic alleles with high

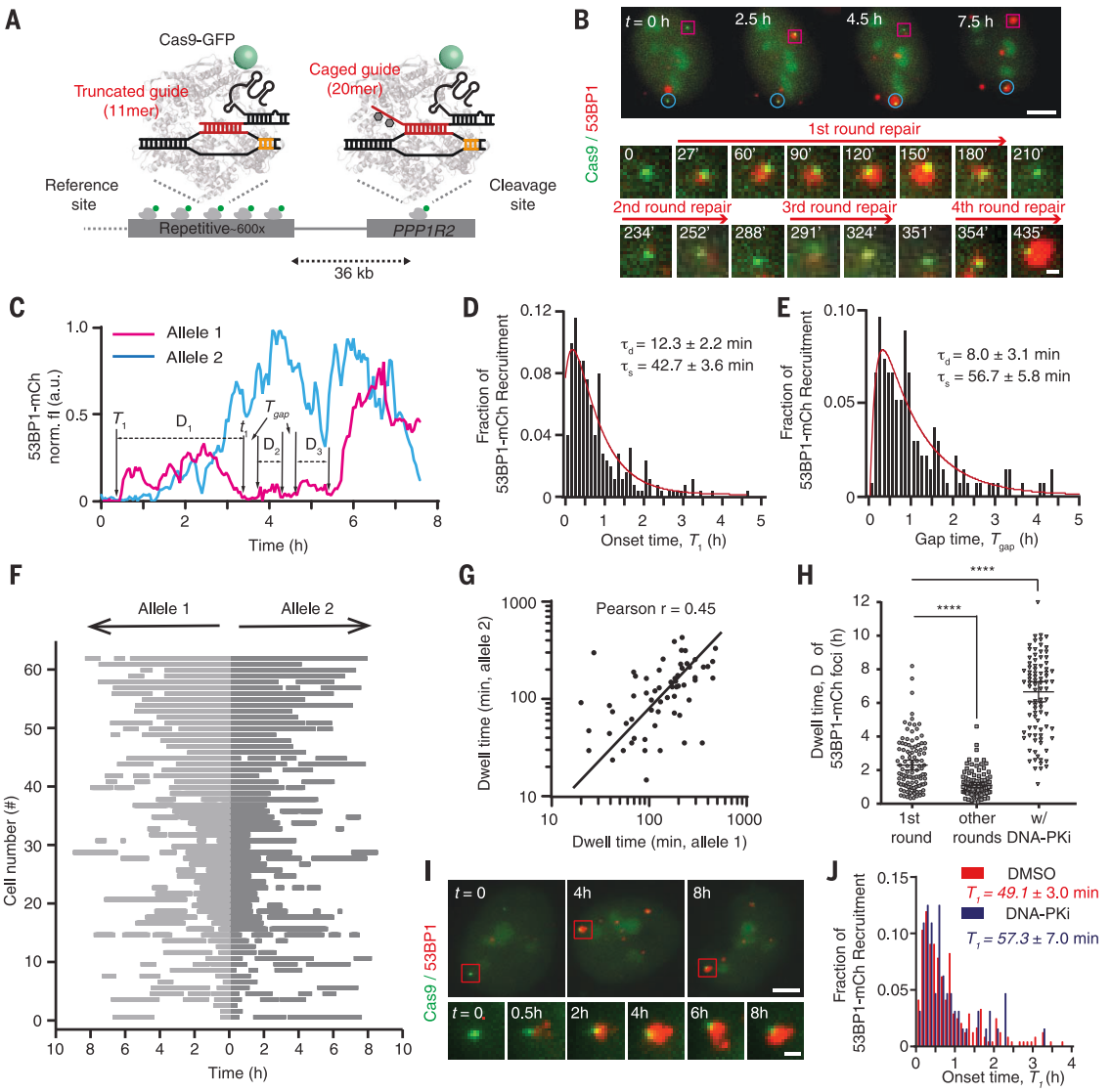

Fig. 3. Live-cell imaging reveals the spatiotemporal dynamics of 53BP1 after synchronized Cas9 DSBs. (**A**) Schematic of orthogonal genomic imaging and cleavage using Cas9-EGFP. (**B**) Snapshots showing 53BP1 recruitment to two different *PPP1R2* alleles (magenta square and cyan circle). Scale bar, 5 μm. Magnified images show multiple cycles of 53BP1 foci at one *PPP1R2* allele (magenta square). Scale bar, 0.7 μm. (**C**) Fluorescence intensity traces of 53BP1-mCherry for both alleles monitored in (B). T_1, t_1, and D_1 denote the start, end, and dwell times for the first cycle of DNA repair, respectively. The time interval T_{gap} is calculated as $T_{n+1} - t_n$ (e.g., $T_2 - t_1$). (**D**) Histogram of initial 53BP1 recruitment time (T_1) at the *PPP1R2* locus after light stimulation. (**E**) Histogram of time interval (T_{gap}) between consecutive 53BP1 cycles for 8 hours. (**F**) Rastergram of 53BP1 foci at 124 paired alleles in 62 cells. Each row displays time courses of 53BP1 foci at a pair of alleles residing in the same nucleus. Gray bars indicate presence of 53BP1-mCherry at each *PPP1R2* allele. Cells are ranked by the mean dwell time of the first 53BP1 recruitment at two alleles (longest to shortest). (**G**) Scatter plot showing positive correlation in dwell time between two alleles in the same cell nucleus ($r = 0.45$). (**H**) Dwell time of 53BP1 foci at *PPP1R2* for the first 53BP1 cycle ($n = 167$ foci in 5 biological replicates), later cycles ($n = 109$ foci in 5 biological replicates), or after DNA-PKcs inhibition (DNA-PKi; $n = 92$ foci in 3 biological replicates). Unpaired t test was performed (****$P < 0.0001$). Error bars indicate 95% confidence interval. (**I**) Snapshots showing longer 53BP1 dwell time in cells with DNA-PKcs inhibition. Scale bars, 5 and 1 μm. (**J**) 53BP1 recruitment time was unchanged ($P > 0.2$) in DNA-PKcs–inhibited cells.

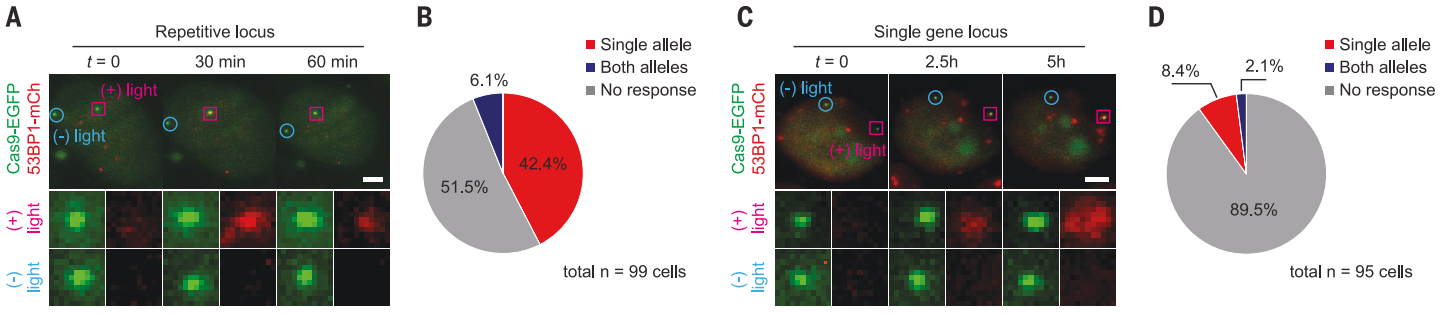

Fig. 4. DSB cleavage at single-allele resolution using subcellular Cas9 activation. (**A**) Single-cell snapshots showing targeted cleavage of Ch3Rep at one of the two alleles (pink). Scale bar, 5 μm. (**B**) Summary of 53BP1-mCh recruitment to Ch3Rep alleles. "Single allele" (red) indicates 53BP1-mCherry recruitment to the targeted allele only; "both alleles" (blue) indicates recruitment to both the targeted and nontargeted alleles; "no response" (gray) indicates no recruitment to either allele ($n = 99$ foci in 4 biological replicates). (**C**) Single-cell snapshots showing targeted cleavage of a single *PPP1R2* allele (pink). Scale bar, 5 μm. (**D**) Summary of 53BP1-mCh recruitment to *PPP1R2* alleles ($n = 95$ foci in 4 biological replicates). Single-allele specificity was calculated by dividing the percentage of monoallelic activation by the percentage of total activation (both monoallelic and biallelic activation). For repetitive cutting (B), this was 42.4/(42.4 + 6.1) × 100 = 87.4%, whereas for single cutting (D), it was 8.4/(8.4 + 2.1) × 100 = 80%.

specificity motivates applications such as simplifying generation of heterozygous mutants (*28*) and potentially reducing and/or eliminating off-target genome editing.

To the best of our knowledge, vfCRISPR provides the highest spatial and temporal resolutions to induce site-specific DSBs in living cells. This study sets the blueprint for further systematic studies of the DDR that combine vfCRISPR with time-resolved biochemical, sequencing, and imaging readouts. The use of cgRNA with other Cas9-based systems such as nickases, base editors, and prime editors may facilitate the study of single-strand break, base excision or mismatch, and flap repair, respectively. Combining vfCRISPR with subcellular photoactivation potentially enables precise genome editing with single-allele specificity and elimination of off-target activity.

REFERENCES AND NOTES

1. G. J. Knott, J. A. Doudna, *Science* **361**, 866–869 (2018).
2. S. E. Polo, S. P. Jackson, *Genes Dev.* **25**, 409–433 (2011).
3. M. van Overbeek *et al*., *Mol. Cell* **63**, 633–646 (2016).
4. B. R. Lemos *et al*., *Proc. Natl. Acad. Sci. U.S.A.* **115**, E2040–E2047 (2018).
5. S. Lin, B. T. Staahl, R. K. Alla, J. A. Doudna, *eLife* **3**, e04766 (2014).
6. E. M. Kallimasioti-Pazi *et al*., *PLOS Biol.* **16**, e2005595 (2018).
7. L. E. Dow *et al*., *Nat. Biotechnol.* **33**, 390–394 (2015).
8. B. Zetsche, S. E. Volz, F. Zhang, *Nat. Biotechnol.* **33**, 139–142 (2015).
9. Y. Nihongaki, F. Kawano, T. Nakajima, M. Sato, *Nat. Biotechnol.* **33**, 755–760 (2015).
10. J. Hemphill, E. K. Borchardt, K. Brown, A. Asokan, A. Deiters, *J. Am. Chem. Soc.* **137**, 5642–5645 (2015).
11. P. K. Jain *et al*., *Angew. Chem. Int. Ed.* **55**, 12440–12444 (2016).
12. J. E. Dahlman *et al*., *Nat. Biotechnol.* **33**, 1159–1161 (2015).
13. D. Singh, S. H. Sternberg, J. Fei, J. A. Doudna, T. Ha, *Nat. Commun.* **7**, 12778 (2016).
14. D. Singh *et al*., *Nat. Struct. Mol. Biol.* **25**, 347–354 (2018).
15. S. H. Sternberg, B. LaFrance, M. Kaplan, J. A. Doudna, *Nature* **527**, 110–113 (2015).
16. H. Lusic, D. D. Young, M. O. Lively, A. Deiters, *Org. Lett.* **9**, 1903–1906 (2007).
17. J. C. Rose *et al*., *Nat. Methods* **14**, 891–896 (2017).
18. B. Wienert *et al*., *Science* **364**, 286–289 (2019).
19. S. Q. Tsai *et al*., *Nat. Biotechnol.* **33**, 187–197 (2015).
20. H. Yin *et al*., *Nat. Chem. Biol.* **14**, 311–316 (2018).
21. E. K. Brinkman *et al*., *Mol. Cell* **70**, 801–813.e6 (2018).
22. R. Aleksandrov *et al*., *Mol. Cell* **69**, 1046–1061.e5 (2018).
23. T. Clouaire *et al*., *Mol. Cell* **72**, 250–262.e6 (2018).
24. B. Chen *et al*., *Cell* **155**, 1479–1491 (2013).
25. H. Ma *et al*., *Nat. Biotechnol.* **34**, 528–530 (2016).
26. H. Wang *et al*., *Science* **365**, 1301–1305 (2019).
27. N. Dimitrova, Y. C. M. Chen, D. L. Spector, T. de Lange, *Nature* **456**, 524–528 (2008).
28. D. Paquet *et al*., *Nature* **533**, 125–129 (2016).

ACKNOWLEDGMENTS

We thank D. Singh for demonstrating initial feasibility on synthetic DNA, B. G. Kang and T. Dawson for selection of the monoclonal U-2 OS cell lines, T. Cottle for helping with in vitro cleavage assays, G. Seydoux for access to the Lonza 4D-Nucleofector, and W. Timp for access to the MiSeq. **Funding:** This work was supported by grants from the National Institutes of Health (R35 GM 122569 to T.H.), the National Science Foundation (PHY 1430124, EFMA 1933303 to T.H. and 1817447 to B.W.), and the Pew Charitable Trust (00030601 to B.W.). R.S.Z. was supported by an NIH Medical Scientist Training Program Award (T32 GM 007309). Y.N. was supported by Japan Society for the Promotion of Science Postdoctoral Fellowships for Research Abroad. This work was also partially supported by NIH GM123130 to Takanari Inoue. T.H. is an investigator of the Howard Hughes Medical Institute. **Author contributions:** Y.L. and T.H. conceived the project. Y.N. and Y.L. demonstrated initial feasibility in mammalian cells. R.S.Z. and Y.L. performed in vitro cleavage assays. R.S.Z., Y.L., and Y.N. performed DSB/indel kinetics measurements. R.S.Z. performed ChIP-seq and GUIDE-seq. Y.L. and S.H. performed immunofluorescence and live-cell imaging. Y.L. and Y.N. developed the monoclonal U-2 OS cell lines. X.L. performed immunoblotting. Y.L., S.R., and S.H. purified SpCas9 proteins. B.W., R.S.Z., and Y.L. developed the theoretical models. Y.L., R.S.Z., B.W., and T.H. wrote the manuscript. T.H. and B.W. supervised the project. **Competing interests:** The authors and Johns Hopkins University have filed a provisional patent application on the method of spatiotemporal control of Cas9 activities through cgRNA. **Data and materials availability:** All data associated with this study are present in the main text or the supplementary materials. All ChIP-seq data have been uploaded to the Sequence Read Archive under BioProject accession PRJNA609749, with analysis code available on GitHub (https://github.com/rogerzou/chipseq_cgRNA). mCherry-BP1-2 pLPC-Pro was obtained from Addgene (#19835) through a material transfer agreement (#39474).

SUPPLEMENTARY MATERIALS

science.sciencemag.org/content/368/6496/1265/suppl/DC1
Materials and Methods
Supplementary Text
Figs. S1 to S26
Tables S1 to S10
References (*29*–*38*)
Movies S1 to S3
MDAR Reproducibility Checklist

View/request a protocol for this paper from *Bio-protocol*.

21 July 2019; resubmitted 29 December 2019
Accepted 14 April 2020
10.1126/science.aay8204

Science

Very fast CRISPR on demand

Yang Liu, Roger S. Zou, Shuaixin He, Yuta Nihongaki, Xiaoguang Li, Shiva Razavi, Bin Wu and Taekjip Ha

Science **368** (6496), 1265-1269.
DOI: 10.1126/science.aay8204

Very fast CRISPR on demand

Numerous efforts have been made to improve the temporal resolution of CRISPR-Cas9–mediated DNA cleavage to the hour time scale. Liu *et al.* developed a Cas9 system that achieved genome-editing manipulation at the second time scale (see the Perspective by Medhi and Jasin). Part of the guide RNA is chemically caged, allowing the Cas9-guide RNA complex to bind at a specific genomic locus without cleavage until activation by light. This fast CRISPR system achieves genome editing at high temporal resolution, enabling the study of early molecular events of DNA repair processes. This system also has high spatial resolution at short time scales, allowing editing of one genomic allele while leaving the other unperturbed.

Science, this issue p. 1265; see also p. 1180

Science (print ISSN 0036-8075; online ISSN 1095-9203) is published by the American Association for the Advancement of Science, 1200 New York Avenue NW, Washington, DC 20005. The title *Science* is a registered trademark of AAAS.